

Observation of a non-local optical response due to motion in an atomic gas with nanoscale thickness

T. Peyrot, Y.R.P. Sortais, J.-J. Greffet, and A. Browaeys
*Laboratoire Charles Fabry, Institut d'Optique Graduate School,
 CNRS, Université Paris-Saclay, F-91127 Palaiseau Cedex, France*

A. Sargsyan
Institute for Physical Research, National Academy of Sciences - Ashtarak 2, 0203, Armenia

J. Keaveney, I.G. Hughes, and C.S. Adams
Department of Physics, Rochester Building, Durham University, South Road, Durham DH1 3LE, United Kingdom

By measuring the transmission of near-resonant light through an atomic vapor with a nanoscale thickness we demonstrate a non-local optical response arising from the motion of atoms with a mean-free path on the order of the cell thickness. Whereas conventional dispersion theory – where the Lorentzian atomic response is simply convolved by the Maxwell-Boltzmann velocity distribution – is unable to reproduce the measured spectra, a model including a non-local susceptibility is found to be consistent with the measurements. This result has important implications for our understanding of light-matter interaction, especially in applications where non-local effects may degrade or enhance the performance of miniaturized atomic sensors.

In elementary treatments of the interaction between matter and electromagnetic fields, one usually assumes a local response of the medium: the polarization vector P at a given position depends only on the value of the electric field E at the same position. For a plane wave illumination of a linear medium, the relation reads: $P(z) = \epsilon_0 \chi(z) E(z)$, where $\chi(z)$ is the susceptibility [1]. However, this assumption of a local response is not always valid and examples exist where it is violated. Among them the low temperature anomalous conductivity of a metal at frequencies ranging from GHz to infra-red [2] is explained by a non-local response, as the skin depth over which the field varies near a surface is smaller than the mean-free path of the electrons in the metal [3, 4]. In the optical domain, excluding non-linear media such as Rydberg ensembles [5], most *linear* bulk media react locally to a field [3, 6]. The situation can be different when confining the field in a region with sub-wavelength size and few experiments observed a non-local response for molecules close to surfaces [7, 8] or in metallic nano-particles [9, 10]. Also, the *selective reflection* at the interface between a glass and an atomic vapor [11–13] was interpreted as an indirect evidence of non-locality as the atoms can travel distances larger than the wavelength of light before colliding, a situation reminiscent of the anomalous skin-depth in metals. Theoretical models were developed where the non-locality is implicit (e.g. [14–18]). Nowadays, atomic vapors confined in nano-cells are considered as potential atomic sensors [18, 19] and ideal media to explore atom-light [20] and atom-surface interactions [21]: it is therefore important to understand the role of non-locality in the optical response of this system.

Here, we observe the non-local optical response of a hot vapor of cesium confined in a nano-cell with a nanoscale thickness by monitoring the *transmission* of a probe laser. We observe that the transmission spectra cannot be reproduced by a model assuming a local susceptibility. We therefore develop theoretical models explicitly non-local. By comparing local and non-local models to the data we conclude that the ob-

served transmission can only be explained by a non-local response arising from atomic motion.

In any homogeneous medium, the relation between the polarization vector and the electric field at a frequency ω is given by (one-dimensional model) [22]:

$$P(z, \omega) = \int_{-\infty}^{+\infty} \epsilon_0 \chi(z - z', \omega) E(z') dz', \quad (1)$$

where $\chi(z - z', \omega)$ is the function describing the spatial response of the cloud, with a decay length ξ called the range of non-locality. To assess whether the optical response is local or non-local, one compares ξ to the length scale over which the electric field varies. Far from any surface, this length scale is the wavelength λ : if $\xi \gtrsim \lambda/2\pi$, the polarization depends on all the values of the field at distances of ξ or less, implying non-locality. By contrast, if $\xi \ll \lambda/2\pi$, the response function is peaked and the optical response is local (see Fig. 1a). In the case of a field confined in a region with a typical size L , such as in a nano-structure or near a metallic surface, the length scale for the variation of the field amplitude is L , and $\xi > L$ leads to a non-local response (see Fig. 1b). However, there translational invariance in the medium is broken due to the presence of the interface and the response function $\chi(z, z', \omega)$ now depends separately on z and z' . In a metallic structure, ξ is often the electron mean free path ($\xi \sim 10 - 100$ nm [3]) and non-local effects arise for $\xi \geq L$, explaining why they have mainly been studied in nano-phonic devices [7–10, 23–25]. For a vapor constituted of atoms moving with a velocity v , the non-locality range corresponds to the atom mean-free path, i.e. the distance travelled by the atomic dipole before it reaches steady-state (due to collisions or radiative decay): $\xi = v/\Gamma_t$ with Γ_t the total homogeneous linewidth [14, 15, 17]. The criterion for non-locality is therefore $v/\Gamma_t \gtrsim \min(\lambda/2\pi, L)$. In large cells, this corresponds to $k_l v/\Gamma_t \gtrsim 1$ ($k_l = 2\pi/\lambda$), or equivalently $\Delta\omega_D/\Gamma_t \gtrsim 1$, with $\Delta\omega_D$ the Doppler width. For

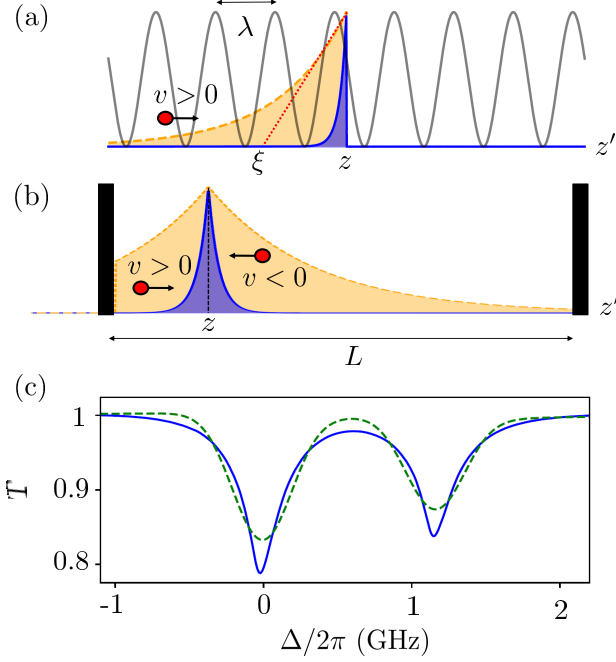


FIG. 1: (a) Illustration of the non-local response of a medium to an electromagnetic field with period λ in free space. Orange fill: non-local response χ for $k_l \xi = k_l v / \Gamma_t = 1.1$; Blue fill: local response χ for $k_l v / \Gamma_t = 0.1$. Black line: field variation amplitude $E = E_0 \cos(k_l z')$ (b) Illustration of the non-local response in presence of an interface in a slab of thickness L . Orange fill: non local response χ for $\xi \sim L$. Blue fill: local response χ for $\xi \ll L$. (c) Blue line: experimental transmission spectrum for $L = 420$ nm and $\Theta \approx 170^\circ\text{C}$ as a function of the laser detuning Δ with respect to the transition $F = 4$ to $F' = 3$. The data are binned 10 times by steps of 2 MHz. The lines correspond respectively to the Cs D1 hyperfine transitions $F = 4$ to $F' = 3$ (left), and $F = 4$ to $F' = 4$ (right). Dashed green line: fit by the first local model.

a thermal vapor of alkali metals $\Delta\omega_D/(2\pi) \sim 200$ MHz and $\Gamma_t/(2\pi) \sim 10$ MHz, yielding $\xi = \Delta\omega_D/(k\Gamma_t) \sim 20/k$, and non-local effects therefore dominate [26]. When the vapor is confined in a nano-cell, as studied here, the optical response is also modified close to the interface (see Fig. 1b), leading to a non-locality that dominates when $\xi \gtrsim L$.

To observe the non-local response of an atomic vapor, we confine a Cs vapor in a wedged sapphire nano-cell of refractive index $n_s = 1.76$, the thickness of which varies from 30 nm to 2 μm [27, 28]. The cell is mounted in a home-made oven that allows differential heating between the reservoir and the windows. The reservoir temperature Θ is monitored by a thermocouple and is related to the atomic density N in the cell via the vapor pressure. An external-cavity diode laser is scanned at 10 Hz around the Cs D1 line at $\lambda = 894$ nm (natural linewidth $\Gamma = 2\pi \times 4.6$ MHz) and we use a 7 cm spectroscopic cell as a reference for frequency calibration. The 700 nW laser beam is focused with an approximate waist of 40 μm and scanned along the wedge to explore various thicknesses L of the atomic slab. We use the back reflec-

tions on the nano-cell to determine L using an interferometric method [29]. Finally, the transmitted light is collected on a photodiode.

When the temperature of the vapor increases, so do the density and the homogeneous linewidth due to collisional dipole-dipole interactions. For $\Theta \geq 250^\circ\text{C}$, we observe linewidths as large as $\Gamma_t = 2\pi \times 1$ GHz leading to $\Delta\omega_D/\Gamma_t \lesssim 0.3$ and $v/(\Gamma_t L) < 1$, thus restoring locality. We used this possibility in our measurement of the collective Lamb shift in a dense vapor [28]. In contrast to that work, here we set the temperature of the vapor to a lower value ($\Theta \approx 170^\circ\text{C}$) to keep the expected homogeneous linewidth $\Gamma_t \approx 2\pi \times 60$ MHz [30] such as $\xi > \max(\lambda/2\pi, L)$, a necessary condition to observe non-local effects. In this case $\Delta\omega_D/\Gamma_t \approx 3$ and $\xi/L > 5$. Operating at a lower temperature would increase these parameters, thus making the non-locality stronger, but at the expense of a much lower absorption, hence reducing the signal-to-noise ratio. The choice of the temperature thus results from a compromise. We present in Fig. 1(c) an example of transmission spectrum, normalized to the value of the signal far from the atomic resonances, for a thickness of the slab $L = 420$ nm. The lineshape appears more complicated than a sum of Gaussian or Lorentzian functions, and we need a model to reveal the influence of the non-locality.

As a first model, we use the dispersion theory relying on a description of the vapor (density N) by a *local* susceptibility χ [1]. Specifically, we calculate χ by summing the contributions of all Doppler-broadened hyperfine transitions of the Cs D1 line at frequencies $\omega_{FF'}$ [31], assuming a normalized Maxwell-Boltzmann velocity distribution $M_v(v)$ along the laser direction of propagation (d is the dipole moment of the strongest transition, $C_{FF'}$ the Clebsch-Gordan coefficients):

$$\chi(\omega) = \frac{Nd^2}{\hbar\epsilon_0} \sum_{F,F'} C_{FF'}^2 \int_{-\infty}^{\infty} \frac{iM_v(v)}{\Gamma_t - 2i(\Delta_{FF'} - k_l v)} dv. \quad (2)$$

Here, $\Delta_{FF'} = \omega - \omega_{FF'} - \Delta_p$ and $\Gamma_t = \Gamma + \Gamma_p$, where we have introduced Δ_p and Γ_p a shift and a broadening characterizing the medium, which originates from the collisional dipole-dipole interactions and the atom-surface interactions [28]. The refractive index is then $n(\omega) = \sqrt{1 + \chi(\omega)}$. We account for the multiple reflections inside the cavity formed by the two sapphire plates (index n_s) surrounding the vapor using the transmission function:

$$t(\omega) = \frac{4n_s n \exp[i(n - n_s)k_l L]}{(n_s + n)^2 - (n_s - n)^2 \exp[2ink_l L]}. \quad (3)$$

Finally, we calculate the normalized transmission $T(\omega) = |t[n(\omega)]/t[n = 1]|^2$. The result of this model is shown in Fig. 1(c), for which we have adjusted the values of N , Δ_p and Γ_p to best fit the data. Strikingly, it does not agree with the data: the experimental linewidth appears narrower than the calculated Doppler broadened width. This is a signature of the coherent Dicke narrowing already observed by many authors [32–35]. In nano-cells, this emphasizes the failure of the

conventional dispersion theory, which assumes a local susceptibility of the atomic gas and a Maxwell-Boltzmann velocity distribution.

In a second model, we introduce the effect of the cell walls in the simplest possible way: we assume that mainly the atoms flying parallel to the walls contribute to the signal, all the others colliding too rapidly with the walls to participate. We therefore take for the velocity distribution $M_v(v) = \delta(v)$ in Eq. 2 [36], to account phenomenologically for the non-locality arising from the surface as explained in the introduction. We fit the data letting as before, N , Δ_P and Γ_P free to evolve. The result, shown in Fig. 2 for $L = 360$ nm is in much better agreement with the data. Nonetheless, the residuals reveal that the model fails to reproduce the narrow feature near resonance, characteristic of the contribution from the fast atoms [13].

Finally, inspired by previous works [17, 37, 38], we derive a third, intrinsically [39] non-local model that accounts both for the explicit k -dependence of the susceptibility and the physics of the atom-surface interaction. To do so we first calculate the response function $\chi(z, z', \omega, v)$. In the presence of interfaces, here the cell walls, this is a challenging task. As is often done [8], we thus treat the atomic medium as homogeneous and model the influence of the surface independently. The susceptibility in the (k, ω) space of an homogeneous gas of atoms with a velocity v is given, for a specific transition, by [40]:

$$\chi_{FF'}(k, \omega, v) = i \frac{d^2 C_{FF'}^2}{\hbar \epsilon_0} \frac{N M_v(v)}{\Gamma_t - 2i(\Delta_{FF'} - kv)}. \quad (4)$$

The k -dependence is at the origin of the non-locality and leads to spatial dispersion [22]. An inverse Fourier transform yields:

$$\chi_{FF'}(z - z', \omega, v) = i N M_v(v) \frac{d^2 C_{FF'}^2}{\hbar \epsilon_0 |v|} e^{(-\frac{\Gamma_t}{2} + i\Delta_{FF'}) \frac{z - z'}{v}} \quad (5)$$

for $(z - z')/v > 0$ and $\chi_{FF'}(z, z', \omega, v) = 0$ for $(z - z')/v < 0$, as required by causality. We recover the decay length $\xi = |v|/\Gamma_t$ introduced above. Finally, the susceptibility of the gas is obtained by summing over all the atomic transitions: $\chi(z, z', \omega, v) = \sum_{F, F'} \chi_{FF'}(z, z', \omega, v)$. As for the influence of the surface, we assume quenching collisions with the cell walls [14], i.e. the atomic dipoles are reset after the collision. We thus account for the breaking of translational invariance in the medium since the coherence is lost at the surface, and velocity classes $\pm v$ are hence independent in contrast to the case of elastic collisions at the wall [40].

To calculate the field transmitted through the cell filled with the vapor, we must also consider the influence of the multiple reflections inside the cavity formed by the sapphire windows (the case of an atomic slab in vacuum is described in [40]). The transmitted field is thus a superposition of the field transmitted by the empty cavity E_{t0} , and of the fields E_{t+} and E_{t-} scattered by the atoms in the forward and backward directions that have undergone multiple reflections before being transmitted. The field transmitted by the empty cavity is $E_{t0} = t_1 t_2 / (1 - r_2^2 e^{2ik_L L}) E_0 e^{ik_L z}$ with $t_1 = 2n_s / (1 + n_s)$,

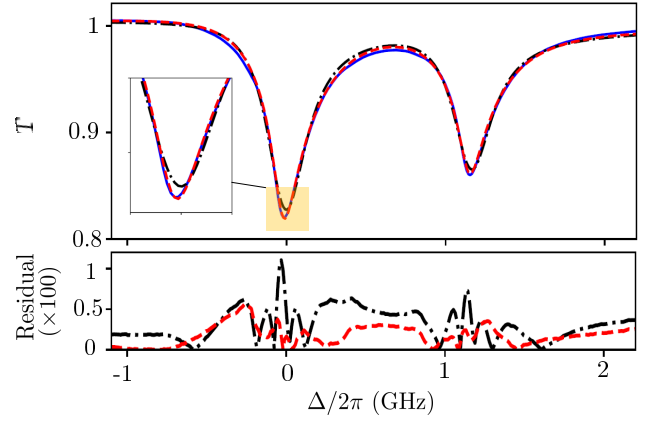


FIG. 2: Top panel. Blue line: experimental transmission spectrum for $\Theta = 170^\circ\text{C}$ and $L = 360$ nm binned as in Fig. 1(c). Black dot-dashed line: fit by the second model. Red dashed line: fit by the third model (see text). Inset: zoom near resonance. Low panel: absolute value of the residuals for both fits.

$t_2 = 2/(1 + n_s)$, $r_2 = (1 - n_s)/(1 + n_s)$ and $E_0 e^{ik_L z}$ the incident field. The fields E_{t+} and E_{t-} are related to the polarization vector $P(z, \omega)$ inside the medium by [40]:

$$E_{t\pm}(z) = \frac{t_2}{1 - r_2^2 e^{2ik_L L}} \frac{ik_L}{2\epsilon_0} \int_0^L dz' P(z', \omega) e^{ik_L(z \mp z')}, \quad (6)$$

where the polarization inside the medium is linked to the *total* cavity field $E(z)$ by:

$$P(z, \omega) = \epsilon_0 \int_{-\infty}^{\infty} dz' \int_{-\infty}^{\infty} dv \chi(z - z', \omega, v) E(z'). \quad (7)$$

The integrals can be calculated provided that the cavity field $E(z')$ is known. This is in general not the case and in the following we assume the atomic medium to be dilute and thin enough so that the cavity field is approximately the one inside the empty cavity (Born approximation [41]): $E(z) \approx t_1 / (1 - r_2^2 e^{2ik_L L}) E_0 [e^{ik_L z} + r_2 e^{ik_L(2L - z)}]$. Under this assumption, we calculate the integrals and, assuming a Maxwell velocity distribution, compute them numerically [40]. Our approach starting from the non-local response function agrees with the formulae obtained in Ref. [38] under the same assumption of dilute and thin medium, i.e. for low absorption.

The data fit by the third model is presented in Fig. 2 for the best found parameters N , Δ_P and Γ_P . The agreement is excellent the narrow feature near resonance are reproduced accurately: despite the fact that we keep the full Maxwell velocity distribution, the velocity selection, imposed in the second phenomenological model and at the origin of the narrowing, is thus automatically included in the third non-local model. To further test the two last models, we also plot in Figs. 3(a,b), the value T_{\min} of the minimum of the transmission for the hyperfine transition from $F = 4$ to $F' = 3$ as a function of the cell thickness. We again observe that both models are in good agreement with the data although the third model fits

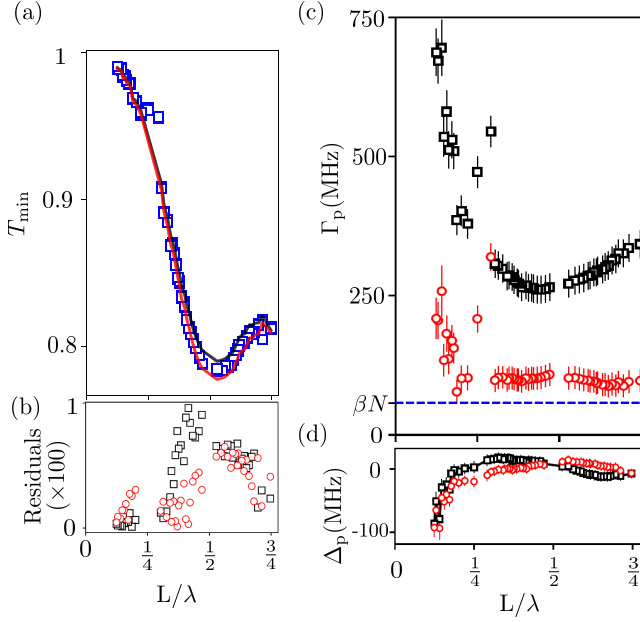


FIG. 3: (a) Minimum of transmission T_{\min} for the transition from $F = 4$ to $F' = 3$ against the cell thickness L . Blue squares: experimental data. Black and red lines: values deduced from the fit of the spectra using the second and third models, respectively. Error bars are smaller than markers. (b) Absolute value of the residuals for the second (black) and third (red) models. (c) (resp. d): broadening parameter Γ_p (resp. shift parameter Δ_p) obtained from the fit of the spectra using the second model (black squares) and third model (red circles). Error bars are the quadratic sum of statistic and fit errors. Blue dotted line: collisional broadening prediction [30].

better around $L \approx \lambda/2$ [42]. We also note that the minimum of transmission does not follow an exponential decay as a function of L , as the Beer-Lambert law would predict. This is expected for two reasons. Firstly, the atoms being in a cavity, the transmitted field amplitude is not given by the Beer-Lambert law but by Eq. (3): a $\lambda/2$ -periodic oscillation, originating from the multiple reflections in the cavity, modulates the exponential decay. Secondly, even without the cavity, the field inside the vapor cannot be exponential due to the non-local character of the medium [14], which leads to a λ -periodic oscillation [40].

Even though the residuals in Fig. 2 could discriminate between the second phenomenological and third non-local models [43], the study of the values of the parameters Δ_p and Γ_p returned by the fit is the clear proof that only the third one is correct. Both parameters characterize the bulk properties of the vapor and the interactions between the atoms and the surfaces. They depend *a priori* on the density N (constant at a given temperature of the vapor) and the cell thickness L . The L -dependence comes only from the atom-surface interaction, as for small L the fraction of atoms close to the surface is larger than for large L . For Cs, the theoretical atom-sapphire interaction coefficient C_3 is around a few $\text{kHz} \cdot \mu\text{m}^3$ [44, 45]: in the range $\lambda/4 \leq L \leq \lambda$ the influence of the surface on

Γ_p and Δ_p is therefore expected smaller than 10 MHz and thus negligible. Importantly, the cavity effects are already taken into account in both models through the multiple reflections and therefore should not contribute to Γ_p and Δ_p [46]. For a fitting model to make sense, it should therefore return values of Γ_p and Δ_p independent of L . Figure 3(c) shows the values of Γ_p returned by the fit for the two last models as a function of L . We observe that only the third model is able to return a value independent of L for $L \geq 200$ nm. At smaller distances, Γ_p increases due to the atom-surface interaction [40]. Furthermore, for $L \geq 200$ nm, Γ_p is in reasonable agreement with the expected broadening βN due to collisional dipole-dipole interactions at the density corresponding to $\Theta \approx 170^\circ\text{C}$ [30]. The second, phenomenological model, by contrast, yields a strong dependence of Γ_p with L , which is not acceptable based on the arguments presented above. As a consequence the only model, which features both a good agreement with the data and a consistent interpretation of its fitting parameters, is the third one. Figure 3(d) presents the fitted Δ_p against L : the difference between the two models is less striking. Both feature the influence of the attractive atom-surface interaction at small thickness.

In conclusion, we have observed that the transmission spectrum of near-resonant light through a slab of cesium vapor can only be understood by a non-local optical response of the medium. In contrast, the local dispersion theory – where the Lorentzian atomic response is simply convolved by the Maxwell velocity distribution – fails to reproduce the data. The non-locality originates from the motion of the atoms and is particularly visible in our experiment owing to the mean-free path being comparable to the cell thickness. Our non-local model makes explicit the non locality by introducing the response function of the vapor. It also assumes a dilute and thin vapor and agrees with the data for extinctions as large as 20%. It would be interesting to explore the cross-over region between the dilute and the dense regimes. Although challenging, extending the non-local model to the dense regime [47] would greatly improve our understanding of matter-light interaction in an unconventional, albeit simple, situation of non-locality in the optical domain.

We thank D. Sarkisyan for discussions. T. Peyrot is supported by the DGA-DSTL fellowship 2015600028. We also acknowledge financial support from CNRS, EPSRC (grant EP/R002061/1) and Durham University. The data presented in this paper will be available later on.

-
- [1] M. Born and E. Wolf, Principles of Optics, Cambridge University Press (1999).
 - [2] A.B. Pippard, The surface impedance of superconductors and normal metals at high frequencies II. The anomalous skin effect in normal metals, *Proc. Roy. Soc. A* **191**, 385 (1947).
 - [3] F. Wooten, Optical properties of solids, Academic, New York (1972).
 - [4] P.W. Gilbert, The anomalous skin effect and the optical prop-

- erties of metals, *J. Phys. F* **12**, 1845 (1982).
- [5] H. Busche, P. Huillery, S.W. Ball, T. Ilieva, M.P.A. Jones, C.S. Adams Contactless nonlinear optics mediated by long-range Rydberg interactions, *Nature Physics*, **13**, 655–658 (2017)
 - [6] Non-local effects are more common in non-linear media, see e.g. R.W. Boyd, *Non-Linear Optics*, 3rd Ed., Academic press; C. Rotschild *et al.*, *Nat. Phys.* **2**, 769 (2006); H. Busche *et al.*, *Nat. Phys.* **13**, 655 (2017).
 - [7] C.F. Eagen, W.H. Weber, S.L. McCarthy and R.W. Therhune, Time-dependent decay of surface-plasmon-coupled molecular fluorescence, *Chem. Phys. Lett.* **75**, 274 (1980).
 - [8] G.W. Ford and W.H. Weber, Electromagnetic interactions of molecules with metal surfaces, *Phys. Rep.* **113**, 195 (1984).
 - [9] U. Kreibig and L. Genzel, Optical absorption of small metallic particles, *J. Phys. Chem. B* **105**, 2264 (2001)
 - [10] Ch. Voisin, N. Del Fatti, D. Christofilos and F. Vallée, Ultrafast electron dynamics and optical nonlinearities in metal nanoparticles, *J. Phys. Chem. B* **105**, 2264 (2001).
 - [11] J.L. Cojan, Contribution à l'étude de la réflexion sélective sur les vapeurs de mercure de la radiation de résonance du mercure, *Ann. Phys* **9**, 385 (1954).
 - [12] A.L.J. Burgmans, M.F.H. Schuurmans and B. Bölger, Transient behavior of optically excited vapor atoms near a solid interface as observed in evanescent wave emission, *Phys. Rev. A* **16**, 5 (1977).
 - [13] S. Briaudeau, S. Saltiel, G. Nienhuis *et al.*, Coherent Doppler narrowing in a thin vapor cell: Observation of the Dicke regime in the optical domain, *Phys. Rev. A* **57**, 5 (1998).
 - [14] M.F.H. Schuurmans, Spectral narrowing of selective reflection, *Journal de Physique* **37**, 469 (1976).
 - [15] G. Nienhuis, F. Schuller and M. Ducloy, Nonlinear selective reflection from an atomic vapor at arbitrary incidence angle, *Phys. Rev. A* **38**, 5197 (1988).
 - [16] T.A. Vartanyan and F. Träger, Line shape of resonances recorded in selective reflection: influence of an antireflection coating, *Opt. Comm.* **110**, 315 (1994).
 - [17] T.A. Vartanyan and D.L. Lin, Enhanced selective reflection from a thin layer of a dilute gaseous medium, *Phys. Rev. A* **51**, 1959 (1995).
 - [18] R. Ritter, N. Gruhler, H. Dobbertin, H. Kübler, S. Scheel, W. Pernice, T. Pfau and R. Löw, Coupling thermal atomic vapor to slot waveguides, *Phys. Rev. X* **8**, 021032 (2018).
 - [19] S. Knappe, P.D.D. Schwindt, V. Shah, L. Hollberg, J. Kitching, L. Liew, and J. Moreland, A chip-scale atomic clock based on ⁸⁷Rb with improved frequency stability, *Opt. Exp.* **13**, 1249 (2005).
 - [20] J. Keaveney, I.G. Hughes, A. Sargsyan, D. Sarkisyan, C.S. Adams Refraction and Superluminal Propagation in a Gaseous Nanolayer *Phys. Rev. Lett.* **109**, 233001 (2012).
 - [21] A. Sargsyan, A. Papoyan, I.G. Hughes, C.S. Adams, and D. Sarkisyan, Selective reflection from an Rb layer with a thickness below $\lambda/12$ and applications, *Opt. Lett.* **42**, 1476 (2017).
 - [22] L.D. Landau, L.P. Pitaevskii and E.M. Lifshitz, *Electrodynamics of continuous media*, Second Edition, Pergamon Press.
 - [23] G.H. Cocoletzi and W.L. Mochán, Excitons: from excitations at surfaces to confinement in nanostructures, *Surf. Sc. Rep.* **57**, 1 (2005).
 - [24] R.J. Churchill and T.G. Philbin, Electromagnetic reflection, transmission, and energy density at boundaries of nonlocal media, *Phys. Rev. B* **94**, 235422 (2016).
 - [25] C. Tserkezis, N. A. Mortensen, and M. Wubs, How nonlocal damping reduces plasmon-enhanced fluorescence in ultranarrow gaps, *Phys. Rev. B* **96**, 085413 (2017).
 - [26] But in large cells, this only leads to a Doppler shift that may be described in the frame of the local conventional dispersion theory.
 - [27] D. Sarkisyan, D. Bloch, A. Papoyan *et al.*, Sub-Doppler spectroscopy by sub-micron thin Cs vapour layer, *Opt. Commun.* **200**, 201 (2001)
 - [28] T. Peyrot, Y.R.P. Sortais, A. Browaeys, A. Sargsyan, D. Sarkisyan, J. Keaveney, I.G. Hughes and C.S. Adams, The collective Lamb Shift of a nanoscale atomic vapour layer within a sapphire cavity, *Phys. Rev. Lett.* **120**, 243401 (2018).
 - [29] E. Jahier, J. Guéna, P. Jacquier, *et al.*, Temperature-tunable sapphire windows for reflection loss-free operation of vapor cells, *Appl. Phys. B* **71**, 561 (2000).
 - [30] L. Weller, R.J. Bettles, P. Siddons, C.S. Adams and I.G. Hughes, Absolute absorption on the rubidium D1 line including resonant dipole-dipole interactions, *J. Phys. B* **44**, 195006 (2011).
 - [31] M.A. Zentile, J. Keaveney, L. Weller, D.J. Whiting, C.S. Adams and I.G. Hughes, ElecSus: A program to calculate the electric susceptibility of an atomic ensemble, *Comp. Phys. Comm.* **189**, 162 (2015).
 - [32] R. Dicke, The effect of collisions upon the Doppler width of spectral lines, *Phys. Rev.* **89**, 472 (1953).
 - [33] R.H. Romer and R. Dicke, New technique for high-resolution microwave spectroscopy, *Phys. Rev.* **99**, 532 (1955).
 - [34] G. Dutier and M. Ducloy, Collapse and revival of a Dicke-type coherent narrowing in a sub-micron thick vapor cell transmission spectroscopy, *Europhys. Lett.* **63**, 35 (2003).
 - [35] A. Sargsyan, Y. Pashayan-Leroy, C. Leroy *et al.*, Collapse and revival of a Dicke-type coherent narrowing in potassium vapor confined in a nanometric thin cell, *J. Phys. B* **49**, 075001 (2016).
 - [36] We also consider in the Supplemental Material [40] the case of a bimodal distribution. The main conclusions of the paper are unchanged, but the price to pay is the introduction of two extra fitting parameters.
 - [37] B. Zambon, G. Nienhuis, Reflection and transmission of light by thin vapor layers, *Opt. Comm.* **143** 308 (1997).
 - [38] G. Dutier and M. Ducloy, Revisiting optical spectroscopy in a thin vapor cell: mixing of reflection and transmission as a Fabry Perot microcavity effect, *J. Opt. Soc. Am. B* **20**, 793 (2003).
 - [39] The model uses the correct constitutive relation between P and E (See Eq. (1)) instead of a macroscopic refractive index such as in the two first models.
 - [40] See Supplemental Material.
 - [41] R. Carminati and J.-J. Greffet, Influence of dielectric contrast and topography on the near field scattered by an inhomogeneous surface, *J. Opt. Soc. Am. A* **12**, 2716 (2003).
 - [42] The odd behavior of the data around $L \simeq \lambda/4$, already pointed out in J. Keaveney *et al.* *Phys. Rev. Lett.* **108**, 173601 (2012) in a different context, is not understood and will be the subject of future investigations.
 - [43] I.G. Hughes and T.P.A. Hase, *Measurements and their Uncertainties: A Practical Guide to Modern Error Analysis* (OUP, Oxford, 2010).
 - [44] K.A. Whittaker, J. Keaveney, I.G. Hughes, A. Sargsyan, D. Sarkisyan and C.S. Adams, Optical response of gas-phase atoms at less than $\lambda/80$ from a dielectric surface, *Phys. Rev. Lett.* **112**, 253201 (2014).
 - [45] D. Bloch and M. Ducloy, Atom-wall interaction, *Adv. Mol. Phys.* **50**, 91 (2005).
 - [46] For the dilute vapor used here, the residual oscillatory dependence of Δ_p with L observed in [28] has an amplitude lower than 10 MHz, and is therefore negligible.
 - [47] G.S. Agarwal, D.N. Pattanayak and E. Wolf, Structure of the electromagnetic field in a spatially dispersive structure, *Phys.*

Rev. Lett. **27**, 1022 (1971).

Supplemental Material: Observation of a non-local optical response due to motion in an atomic gas with nanoscale thickness

T. Peyrot, Y.R.P. Sortais, J.-J. Greffet, and A. Browaeys
*Laboratoire Charles Fabry, Institut d'Optique Graduate School,
 CNRS, Université Paris-Saclay, F-91127 Palaiseau Cedex, France*

A. Sargsyan
Institute for Physical Research, National Academy of Sciences - Ashtarak 2, 0203, Armenia

J. Keaveney, I.G. Hughes, and C.S. Adams
*Department of Physics, Rochester Building, Durham University,
 South Road, Durham DH1 3LE, United Kingdom*

In this Supplemental Material, we first derive the equations of the third (non-local) model of the main text used in the main text. In Section II, we show that using a bimodal velocity distribution in the second model of the main text cannot reproduce consistently the data either. In Section III we give more details about the deviation of the transmission coefficient from the Beer-Lambert law. Finally, we analyze in more details the thickness dependence of the parameter Γ_p extracted from the fit of the data by the local model.

I. DERIVATION OF THE NON-LOCAL MODEL

In this first Section, we derive the expression of the transmission through the atomic slab, including the cavity effect from the sapphire plates of the nanocell, making explicit the origin of the non-locality.

A. The non-local susceptibility

We start by deriving the expression of the non-local susceptibility $\chi(z, z', \omega, v)$ of the ensemble of atoms for a velocity class v and at frequency ω . As explained in the main text, the presence of the cell walls makes it a challenging task in general. To simplify the situation, we will use the following procedure:

1. We will treat the vapor as if it was homogeneous (i.e. in the absence of confining walls). In this case, the susceptibility depends only on the difference: $\chi(z, z', \omega, v) = \chi(z - z', \omega, v)$.
2. We will treat the effect of the surface separately. This will be done by assuming quenching collisions at the cell walls, i.e. the atomic coherence will be lost during these collisions [1] and reset to zero. In this way, there will not exist any relation between the coherence of atoms moving at $+v$ or $-v$, contrarily to what would happen if the collisions with the walls were elastic.

To derive the susceptibility for an homogeneous vapor, we first consider a given atomic transition between ground and excited states F and F' (frequency $\omega_{FF'}$, and total homogeneous linewidth Γ_t) described by a coherence ρ_{12} and

a dipole matrix element $d_{FF'} = C_{FF'} d$ ($C_{FF'}$ is the Clebsch Gordan coefficient normalized to the strongest transition with dipole moment d). We introduce the coherence field $\rho_{12}(z, t, v)$ at position z in the slab for the velocity class v . In the low intensity limit (i.e. neglecting populations in the excited state), the Maxwell-Bloch equation for the coherence is:

$$\frac{d\rho_{12}(z, t, v)}{dt} = -i\omega_{FF'}\rho_{12}(z, t, v) + iC_{FF'}\frac{dE(z, t)}{2\hbar} - \frac{\Gamma_t}{2}\rho_{12}(z, t, v). \quad (1)$$

Using the convective derivative $d/dt = \partial/\partial t + v\partial/\partial z$, we get:

$$\frac{\partial\rho_{12}(z, t, v)}{\partial t} + v\frac{\partial\rho_{12}(z, t, v)}{\partial z} = -i\omega_{FF'}\rho_{12}(z, t, v) + iC_{FF'}\frac{dE(z, t)}{2\hbar} - \frac{\Gamma_t}{2}\rho_{12}(z, t, v). \quad (2)$$

Taking the Fourier transform of this equation with respect to t and z we obtain:

$$\rho_{12}(k, \omega, v) = iC_{FF'}\frac{dE(k, \omega)}{2\hbar} \frac{1}{\Gamma_t/2 - i(\Delta_{FF'} - kv)}, \quad (3)$$

with $\Delta_{FF'} = \omega - \omega_{FF'}$. In the (k, ω) space and for an *homogeneous medium*, the relation between the polarization and the field is: $P(k, \omega, v) = \epsilon_0\chi(k, \omega, v)E(k, \omega)/2$. The factor 2 appears here to be compatible with the relation valid for a local medium using complex notation: $P = \epsilon_0\chi\frac{E}{2} + \text{c.c.}$ Furthermore, in the dilute approximation, $P(k, \omega, v) = NM_v(v)dC_{FF'}\rho_{12}(k, \omega, v)$, with N the density of the vapor and $M_v(v)$ the normalized velocity distribution. Consequently the susceptibility of the vapor in the (k, ω) space is:

$$\chi(k, \omega, v) = iNM_v(v)\frac{C_{FF'}^2d^2}{\hbar\epsilon_0} \frac{1}{\Gamma_t/2 - i(\Delta_{FF'} - kv)}. \quad (4)$$

This susceptibility depends explicitly on k and this is the reason for the non-local response of the medium (i.e. the spatial dispersion). We note that this approach using a convective derivative is similar to the one used to derive the permittivity of a metal in the anomalous skin-depth situation [2]. The inverse Fourier transform in k yields the susceptibility:

$$\chi(z - z', \omega, v) = iNM_v(v)\frac{C_{FF'}^2d^2}{\hbar\epsilon_0} \frac{1}{2\pi} \int_{-\infty}^{\infty} \frac{e^{ik(z-z')}}{\Gamma_t/2 - i(\Delta_{FF'} - kv)} dk. \quad (5)$$

To calculate the integral, we integrate in the k -complex plane. When applying the residue theorem, care must be taken, as the position of the pole $k_0 = (\Delta_{FF'} + i\Gamma_t/2)/v$ in the plane depends on the sign of the velocity. We obtain the non-local response function presented in the main text [Eq.(5)]:

$$\chi(z - z', \omega, v) = 0 \quad \text{when} \quad \frac{z - z'}{v} < 0, \quad (6)$$

$$\chi(z - z', \omega, v) = iNM_v(v)\frac{C_{FF'}^2d^2}{\hbar\epsilon_0|v|} \exp\left[\left(-\frac{\Gamma_t}{2} + i\Delta_{FF'}\right)\frac{z - z'}{v}\right] \quad \text{when} \quad \frac{z - z'}{v} > 0. \quad (7)$$

The expression (7) shows that the distance ξ over which the polarization depends on the field (i.e. the range of non-locality) is $\xi = |v|/\Gamma_t$, thus confirming the qualitative discussion in the main text. Furthermore the fact that $\chi(z - z', \omega, v)$ depends on the sign of $(z - z')/v$ indicates that the optical response at position z only depends on atoms located at position $z' < z$ moving with a positive velocity and on atoms at $z' > z$ having a negative velocity.

B. Transmitted field for a dilute slab placed in vacuum

We first consider an atomic slab of thickness L placed in vacuum, i.e. we do not consider the sapphire windows of the nano-cell. The slab is excited by a plane wave (frequency ω) with complex amplitude $E_0 \exp[ik_l z]$ where $k_l = \omega/c$.

Using the superposition principle, the amplitude of the field transmitted after the slab is [3, 4]:

$$E_t(z > L) = E_0 e^{ik_l z} + \frac{ik_l}{2\epsilon_0} \int_0^L dz' P(z', \omega) e^{ik_l(z-z')} . \quad (8)$$

In a non-local linear medium consisting of atoms moving with velocity v (distribution $M_v(v)$) as considered here, the relation between the polarization vector and the field is:

$$P(z, \omega) = \int_{-\infty}^{\infty} dz' \int_{-\infty}^{\infty} dv \epsilon_0 \chi(z - z', \omega, v) M_v(v) E(z') dz' , \quad (9)$$

leading to the following expression for the transmitted field:

$$E_t = E_0 e^{ik_l z} + \frac{ik_l}{2\epsilon_0} \int_0^L dz' e^{ik_l(z-z')} \left[\int_{-\infty}^{\infty} dz'' \epsilon_0 \left(\int_{-\infty}^{\infty} dv \chi(z' - z'', \omega, v) M_v(v) \right) E(z'') \right] . \quad (10)$$

Considering the geometry of the slab, the integral over z'' is bounded between 0 and L . Using the expression of the non-local susceptibility (7), the second term of (10) is a sum of two integrals:

$$I_0 = \frac{ik_l}{2\epsilon_0} \int_0^L dz' e^{ik_l(z-z')} \left[\int_0^{z'} dz'' \epsilon_0 \left(\int_0^{\infty} dv \frac{iNC_{FF'}^2 d^2}{\hbar \epsilon_0 v} e^{\frac{z'-z''}{v}(-\frac{\Gamma_t}{2} + i\Delta_{FF'})} M_v(v) \right) E(z'') \right] \quad (11)$$

$$I'_0 = \frac{ik_l}{2\epsilon_0} \int_0^L dz' e^{ik_l(z-z')} \left[\int_{z'}^L dz'' \epsilon_0 \left(\int_{-\infty}^0 dv \frac{-iNC_{FF'}^2 d^2}{\hbar \epsilon_0 v} e^{\frac{z'-z''}{v}(-\frac{\Gamma_t}{2} + i\Delta_{FF'})} M_v(v) \right) E(z'') \right] . \quad (12)$$

The fact that we can separate the integral in Eq. (10) into two integrals, one involving negative velocities, and the other positive ones, using Eqs. (6) and (7) for $\chi(z - z', \omega, v)$ comes from the second hypothesis at the beginning of Sec. I A: we assume that the atoms lose their coherence at the boundaries of the slab. Otherwise, an atom with a velocity $-v$ would bounce off the surface, switching its velocity to $+v$, and would contribute to the polarization even for $z' < z$.

In order to proceed further, we need the expression of the field inside the vapor. As we consider a dilute atomic medium placed in vacuum, we neglect the reflection at the boundaries of the slab and take $E(z'') \approx E_0 \exp[ik_l z'']$. The integrals I_0 and I'_0 become respectively:

$$I_0 = -\frac{NC_{FF'}^2 d^2}{2\hbar \epsilon_0} E_0 \exp[ik_l z] \int_0^{\infty} dv M_v(v) \left(\frac{k_l L}{\Lambda} + \frac{k_l v e^{-\frac{\Lambda L}{v}}}{\Lambda^2} - \frac{k_l v}{\Lambda^2} \right) , \quad (13)$$

$$I'_0 = -\frac{NC_{FF'}^2 d^2}{2\hbar \epsilon_0} E_0 \exp[ik_l z] \int_{-\infty}^0 dv M_v(v) \left(\frac{k_l L}{\Lambda} - \frac{k_l v e^{\frac{\Lambda L}{v}}}{\Lambda^2} + \frac{k_l v}{\Lambda^2} \right) , \quad (14)$$

where we have introduced, as in Ref. [5], $\Lambda = \Gamma_t/2 - i(\Delta_{FF'} - k_l v)$. Combining Eqs. (10), (13) and (14), the final expression of the field transmitted after the slab is:

$$E_t = E_0 e^{ik_l z} \left[1 - \frac{NC_{FF'}^2 d^2}{2\hbar \epsilon_0} \int_{-\infty}^{\infty} dv M_v(v) \left(\frac{k_l L}{\Lambda} - \frac{k_l |v|}{\Lambda^2} + \frac{k_l |v| e^{-\frac{\Lambda L}{|v|}}}{\Lambda^2} \right) \right] , \quad (15)$$

Equation (15) is equivalent to the one derived by several authors [5, 6] starting from a different point of view, which made the non-locality less explicit than the above derivation. We now discuss the contributions of the three integrals (labeled J_1, J_2 and J_3 respectively) in Eq. (15) (see also [5]). We first note that in this discussion, we will have to consider three length scales: the non-locality distance ξ , the reduced wavelength of the light $1/k_l$, and the thickness of the slab L .

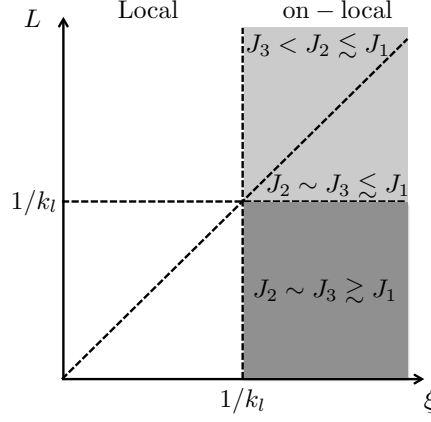


FIG. 1: Contribution of the three integrals J_1, J_2 and J_3 in Eq.(15) as a function of the non-locality distance ξ and the cell thickness L . The regime explored in this work lies in the lower right corner.

1. The first term J_1 is the one we would have obtained had we simply taken for the susceptibility $\chi(z, z', \omega, v)$ of the vapor the (incorrect!) expression:

$$\chi(z - z', \omega, v) = i \frac{NC_{FF'}^2 d^2}{\hbar \epsilon_0} \frac{1}{\Gamma_t/2 - i(\Delta_{FF'} - k_l v)} \delta(z - z') \quad (16)$$

where the detuning $\Delta_{FF'}$ is replaced by $\Delta_{FF'} - k_l v$. Although intuitive, this approach would have missed the contributions from the two remaining terms. This term J_1 dominates as soon as $L \gtrsim |v/\Lambda|$. We consider two cases: (i) far from resonance ($\Delta_{FF'} \gg \Gamma_t, \Delta\omega_D$), J_1 dominates when $L \gg \Delta\omega_D/(k_l \Delta)$, and (ii) near resonance ($\Delta_{FF'} = 0$), J_1 dominates when $L \gtrsim 1/k_l$. This indicates that in large cells ($L \gtrsim 1 \mu\text{m}$), J_1 is the dominant contribution and the conventional dispersion theory applies.

2. The second and third terms J_2 and J_3 become important as soon as $|v|/(|\Lambda|L) \gtrsim 1$, i.e. $L \lesssim 1/k_l$. They are a consequence of the non-local character of the atomic response and have an influence for thin cells, hence justifying the use of a nano-cell in the experiment.
3. Finally, the third term $J_3 \sim J_2 \exp[-L/\xi]$ describes the fact that the atomic dipole stops emitting when it reaches the boundary of the slab. When $J_2 \gtrsim J_1$, we have seen that $L < 1/k_l$ near-resonance ($\Delta_{FF'} = 0$). As $\xi > 1/k_l$ in the non-local regime, $L < \xi$ and $J_3 \sim J_2$, indicating that in the non-local regime it is not possible that J_2 alone dominates.

Figure 1 summarizes the various regimes as a function of the values of L and ξ . The important message is that in large ensembles (i.e. $L > 1/k_l$), the standard dispersion theory holds by simply replacing in the steady state susceptibility the detuning $\Delta_{FF'}$ by $\Delta_{FF'} - k_l v$ and integrating over the velocity distribution. This is already non-local as soon as $\xi \geq 1/k_l$, or $\Delta\omega_D \gtrsim \Gamma_t$. However the non-locality appears more strikingly in small systems, where $L \lesssim \xi$ and $L \lesssim 1/k_l$: there two extra terms sign unambiguously the non-local character of the atomic response.

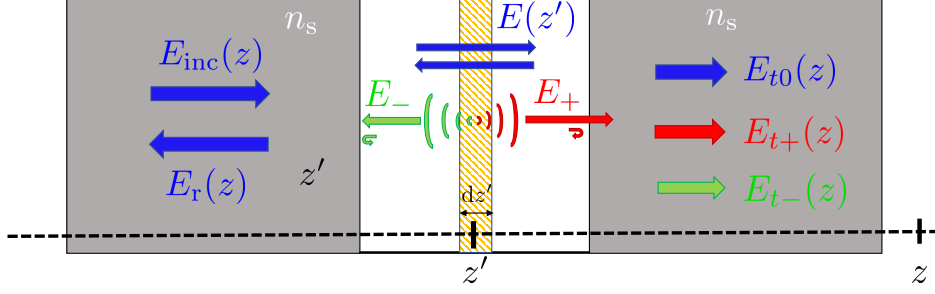


FIG. 2: Configuration used to calculate the transmission through the cell. The dilute vapour is confined between two sapphire plate of index n_s . The incident field $E_0 \exp[ik_l z]$ undergoes multiple reflections inside the cell before being finally transmitted (E_{t0}). The field $E(z')$ inside the cell excite the atoms in the slice dz' , and radiate a field in the forward (backward) direction E_+ (E_-) that is reflected multiple times before leading to the transmitted fields E_{t+} (E_{t-}).

C. Transmitted field in a dilute regime with cavity boundaries

We now consider the more involved case where the atomic slab is confined between the two windows of the cell (index n_s), leading to a pronounced cavity effect. This situation has already been discussed, in particular in Ref. [7] starting from a different point of view. Here we use the non-local susceptibility given by Eq.(7) to derive the transmission of the slab confined in the nanocell.

Figure 2 summarizes the different fields involved. First, we need to consider the field inside the empty cavity between the two windows, which reads:

$$E(z'') = \frac{E_0 t_1}{1 - r_2^2 e^{2ik_l L}} \left(e^{ik_l z''} + r_2 e^{ik_l (2L - z'')} \right) \quad (17)$$

with $t_1 = 2n_s/(1 + n_s)$ and $r_2 = (1 - n_s)/(1 + n_s)$. Second, the field emitted by the atoms of the vapor also undergoes multiple reflections on the cavity walls. We separate this field into two components propagating respectively in the forward and backward directions and consider the multiple reflections of each. Consequently, the field transmitted after the cell results from the interference of (i) the field $E_{t0} = \frac{t_1 t_2}{1 - r_2^2 e^{2ik_l L}} E_0 e^{ik_l z}$ of the cavity without any atoms, (ii) the field E_{t+} emitted by all slices dz' initially directed in the forward direction and undergoing multiple reflections, and (iii) the field E_{t-} initially emitted in the backward direction, also undergoing reflections. The transmitted field is therefore:

$$E_t(z) = \frac{t_1 t_2}{1 - r_2^2 e^{2ik_l L}} E_0 e^{ik_l z} + E_{t+}(z) + E_{t-}(z), \quad (18)$$

with $t_2 = 2/(n_s + 1)$. The field emitted by the atoms in the forward direction is, taking into account the non-local relation between $P(z)$ and $E(z)$ inside the vapor:

$$E_{t+} = A \frac{ik_l}{2\epsilon_0} \int_0^L dz' e^{ik_l(z-z')} \left[\int_{-\infty}^{\infty} dz'' \epsilon_0 \left(\int_{-\infty}^{\infty} dv \chi(z' - z'', \omega, v) M_v(v) \right) E(z'') \right] \quad (19)$$

with

$$A = t_2(1 + r_2^2 e^{2ik_l L} + r_2^4 e^{4ik_l L} + \dots) = \frac{t_2}{1 - r_2^2 e^{2ik_l L}} \quad (20)$$

the prefactor that accounts for the multiple reflections before the field exits the cavity. To calculate the integral we again assume a dilute vapor and use the expression (17) valid for an empty cavity. Calculations similar to the ones performed for the slab immersed in vacuum (Sec.IB) lead to:

$$E_{t+} = ABC (I_1 + I_2) E_0 \exp[ik_l z] \quad (21)$$

with

$$I_1 = - \int_0^\infty dv M_v(v) \left[\frac{L}{\Lambda_+} + \frac{v}{\Lambda_+^2} e^{-\Lambda_+ \frac{L}{v}} - \frac{v}{\Lambda_+^2} + \frac{r_2 e^{2ik_l L}}{\Lambda_-} \left(\frac{1}{2ik_l} (1 - e^{-2ik_l L}) + \frac{v}{\Lambda_+} (e^{-\Lambda_+ \frac{L}{v}} - 1) \right) \right], \quad (22)$$

and

$$I_2 = \int_{-\infty}^0 dv M_v(v) \left[-\frac{L}{\Lambda_+} + \frac{v}{\Lambda_+^2} e^{\Lambda_+ \frac{L}{v}} - \frac{v}{\Lambda_+^2} + \frac{r_2 e^{2ik_l L}}{\Lambda_-} \left(\frac{1}{2ik_l} (e^{-2ik_l L} - 1) + \frac{v}{\Lambda_+} e^{\Lambda_+ \frac{L}{v}} (1 - e^{-\Lambda_+ \frac{L}{v}}) \right) \right], \quad (23)$$

where we have introduced $\Lambda_\pm = \Gamma_t/2 - i(\Delta_{FF'} \mp k_l v)$, $B = t_1/(1 - r_2^2 e^{2ik_l L})$ and $C = NC_{FF'}^2 d^2 k_l / (2\hbar\epsilon_0)$.

We proceed in a similar way for the field E_{t-} initially emitted in the backward direction, noting that the polarization vector at position z' due to the backward emitted field is retarded by a factor $r_2 e^{2ik_l z'}$ (see Fig. 2). We get:

$$E_{t-} = Ar_2 \frac{ik_l}{2\epsilon_0} \int_0^L dz' e^{ik_l(z+z')} \left(\int_{-\infty}^\infty dz'' \epsilon_0 \left[\int_{-\infty}^\infty dv \chi(z' - z'', \omega, v) M_v(v) \right] E(z'') \right). \quad (24)$$

This leads to:

$$E_{t-} = r_2 ABC (I_3 + I_4) E_0 \exp[ik_l z] \quad (25)$$

with

$$I_3 = - \int_0^\infty dv M_v(v) \left[\frac{1}{\Lambda_+} \left(\frac{e^{2ik_l L} - 1}{2ik_l} + \frac{v}{\Lambda_-} (e^{-\Lambda_- \frac{L}{v}} - 1) \right) + \frac{r_2 e^{2ik_l L}}{\Lambda_-} \left(L + \frac{v}{\Lambda_-} (e^{-\Lambda_- \frac{L}{v}} - 1) \right) \right] \quad (26)$$

and

$$I_4 = \int_{-\infty}^0 dv M_v(v) \left[\frac{1}{\Lambda_+} \left(\frac{1 - e^{2ik_l L}}{2ik_l} + \frac{v}{\Lambda_-} (e^{\Lambda_- \frac{L}{v}} - e^{2ik_l L}) \right) + \frac{r_2 e^{2ik_l L}}{\Lambda_-} \left(-L + \frac{v}{\Lambda_-} (e^{\Lambda_- \frac{L}{v}} - 1) \right) \right]. \quad (27)$$

Finally, the transmitted field is:

$$E_t(z) = \left(\frac{t_1 t_2}{1 - r_2^2 e^{2ik_l L}} + ABC [I_1 + I_2 + r_2 (I_3 + I_4)] \right) E_0 \exp[ik_l z]. \quad (28)$$

We retrieve the expression obtained in Ref. [7] using a different approach. Here again, the fact that in Eqs.(19) and (24) we can separate the integral into two integrals involving only the positive [Eqs.(22) and (26)] or the negative velocities [Eqs.(23) and (27)] comes from the assumptions that the atomic coherences are lost in a quenching collisions at the cell walls.

D. Case of a multilevel atom

So far we have considered a single atomic transition. In the experiment, several hyperfine transitions of the D1 cesium line contribute. In order to account for them we calculate the susceptibility by summing over all transitions and Eqs. (15) and (28) respectively become:

$$E_t = E_0 e^{ik_l z} \left[1 - \sum_{FF'} \frac{NC_{FF'}^2 d^2}{4\hbar\epsilon_0} \int_{-\infty}^{\infty} dv M_v(v) \left(\frac{k_l L}{\Lambda} - \frac{k_l |v|}{\Lambda^2} + \frac{k_l |v| e^{-\frac{\Lambda L}{|v|}}}{\Lambda^2} \right) \right], \quad (29)$$

$$E_t(z) = \left(\frac{t_1 t_2}{1 - r_2^2 e^{2ik_l L}} + \sum_{FF'} ABC [I_1 + I_2 + r_2(I_3 + I_4)] \right) E_0 \exp[ik_l z], \quad (30)$$

where the detuning appearing in Λ is $\Delta_{FF'} = \omega - \omega_{FF'}$.

II. BIMODAL VELOCITY DISTRIBUTION

At the end of the main text, we compare two models: a phenomenological model where we use the local susceptibility, but modify the velocity distribution to account for the non locality due to the interface, taking $M_v(v) = \delta(v)$, and the more accurate non-local model derived in Sec.I. We conclude that the second non-local model is able to explain the data in a more satisfactory way, as it yields a linewidth Γ_p independent of L . We show here that the use of a more refined velocity distribution in phenomenological model does not affect this conclusion.

To do so, we use a bimodal normalized velocity distribution, already introduced in the context of nano-cells [8]:

$$M_v(v) = W \left(a \exp \left[-\frac{v^2}{u^2} \right] + (1 - a) \exp \left[-\left(\frac{v}{su} \right)^2 \right] \right), \quad (31)$$

where $u = \sqrt{2k_B T/M}$ is the root-mean square velocity and $W = (au\sqrt{\pi} + (1-a)su\sqrt{\pi})^{-1}$. The additional parameters a and s describe respectively the fraction of slow atoms and the width of the component of the distribution corresponding to the fast atoms. This bimodal distribution therefore consists in a pedestal associated to the slow atoms and a sharp feature superimposed on coming from the fast atoms. We fit the data using this velocity distribution in the local model with N , Γ_p , Δ_p , a and s as free parameters. The result is shown in Fig. 3 as green squares. Similarly to the case where $M_v(v) = \delta(v)$, the strong dependence of Γ_p with L is not compatible with a physical interpretation.

III. DEVIATION FROM BEER-LAMBERT TRANSMISSION LAW

Figures 3(a,b) of the main text show that the minimum of transmission of the hyperfine transition $F = 4$ to $F' = 3$ does not follow the Beer-Lambert law. To gain further insight on this behavior, we study the evolution of the minimum of the theoretical transmission T_{\min} as a function of the vapor thickness L . To separate the effect of the cavity from the one of the non-local response, we consider two models: (i) the first local model of the text that accounts for the cavity (Eq. (3) of main text) with a local index of refraction. (ii) the non-local model, but without the cavity surrounding the atomic (Eq. (18) of the Supplemental Material). The results are shown in Fig. 4. We observe that

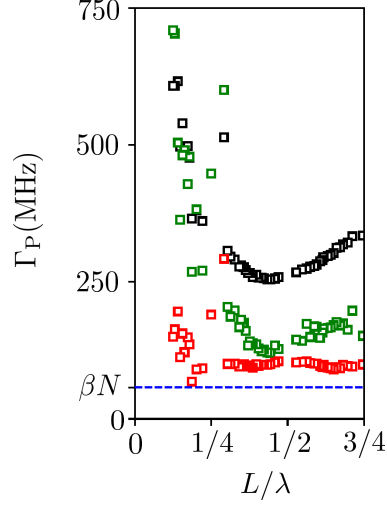


FIG. 3: Fitted broadening parameter Γ_p versus the cell thickness L . Black squares: phenomenological model where we use the local susceptibility with $M_v(v) = \delta(v)$. Green squares: same using the bimodal velocity distribution. Red squares: accurate non-local model as derived in Sec. I.

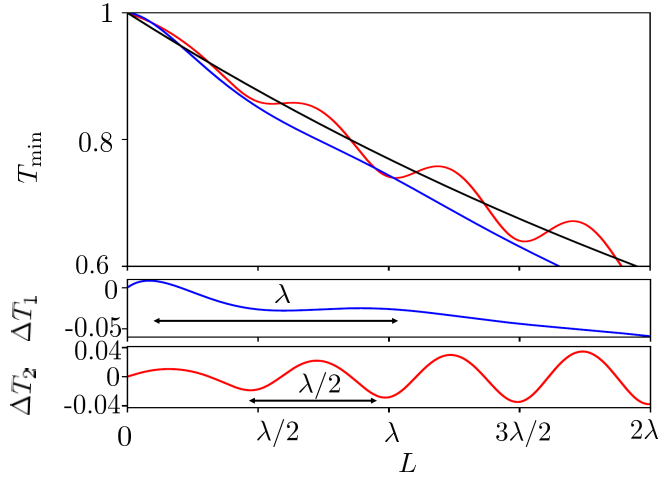


FIG. 4: Top : Minimum of the transmission, T_{\min} , versus L extracted from the local model including the cavity (red line) and from the non-local model without any cavity surrounding the slab (blue line). Black line : prediction of the Beer-Lambert law. Parameters used : $\Delta_p = 0$, $\Gamma_p = 2\pi \times 100$ MHz and $\Theta = 188^\circ\text{C}$. Bottom : deviations of the non-local (ΔT_1) and local (ΔT_2) models from the Beer Lambert law.

the cavity surrounding a local-medium leads to an oscillation of T_{\min} with L with a period $\lambda/2$, as it should for a standing wave in a cavity. The non-local response of the cloud results into an oscillation of T_{\min} with a period λ . This can also be seen from Eq. (15) where the last term $\exp[-\Lambda L/|v|]$ leads to an oscillatory dependence in $k_l L$.

IV. THICKNESS DEPENDENCE OF Γ_p IN THE PHENOMENOLOGICAL SECOND MODEL

In Fig.3(c) of the main text, we observe a strong dependence of the broadening parameter Γ_p with the thickness L for the phenomenological model. In this section we deconvolve the effects of the Casimir atom-surface interaction

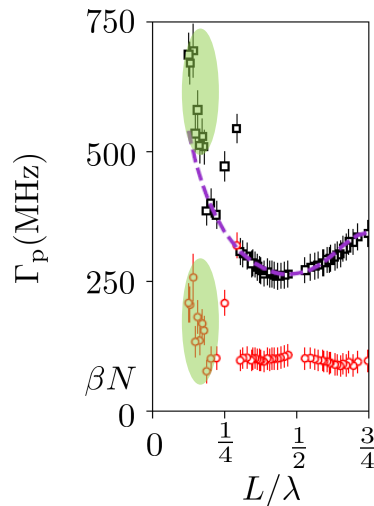


FIG. 5: Broadening parameter Γ_p obtained from the fit of the experimental spectra using the *phenomenological second* model of the main text (black squares) and the non-local model of Sec. I (red circles). Error bars are the quadratic sum of statistic and fit errors. The violet dashed line is the broadening parameter Γ_p obtained from the fit using the phenomenological non-local model of the data simulated by the expression derived in Sec. IC. Green shaded areas indicate the region where the Casimir atom-surface interactions dominate the broadening.

from the non-local influence of the surface when $\xi \geq L$ on the parameter Γ_p returned by the fit. To understand the sharp increase for small L , we simulate a collection of spectra with the accurate non-local model of Sec. I for a fixed temperature ($\Theta = 170^\circ\text{C}$), a fixed broadening $\Gamma_p = 100$ MHz and various L between $\lambda/8$ and $3\lambda/4$. We do not include the Casimir atom-surface interaction in the model. We then fit each generated spectra by the *phenomenological* model and extract the corresponding Γ_p . The result is shown as a violet dashed line in Fig. 5.

We observe a very good agreement of the fitted Γ_p for the experimental and simulated data using the accurate non-local model for $L \gtrsim 150$ nm. This indicates that the increase of Γ_p at small L is a feature of the phenomenological, non-local model. The sharper increase for $L \leq 150$ nm is therefore ascribed to the Casimir atom-surface interactions, and can also be seen in the variation of Γ_p returned by the accurate non-local model with L .

-
- [1] M.F.H. Schuurmans, Spectral narrowing of selective reflection, *Journal de Physique* **37**, 469 (1976).
 - [2] P.W. Gilbert, The anomalous skin effect and the optical properties of metals, *J. Phys. F* **12**, 1845 (1982).
 - [3] H. Fearn, D.F.V. James and P. Milonni, Microscopic approach to reflection, transmission and the Ewald-Osen extinction theorem, *Am. J. Phys.* **64**, 986 (1996).
 - [4] R.P. Feynman, R.B. Leighton and M. Sands, *Lectures on Physics*, vol. 1, chap. 30, Addison Wesley (2006).
 - [5] S. Briaudeau *et. al*, Coherent Doppler narrowing in a thin vapor cell: Observation of the Dicke regime in the optical domain, *Phys. Rev. A* **57**, 5 (1998).
 - [6] T.A. Vartanyan and D.L. Lin, Enhanced selective reflection from a thin layer of a dilute gaseous medium, *Phys. Rev. A* **51**, 1959 (1995).
 - [7] G. Dutier and M. Ducloy, Revisiting optical spectroscopy in a thin vapor cell: mixing of reflection and transmission as a Fabry Perot microcavity effect, *J. Opt. Soc. Am. B* **20**, 793 (2003).

- [8] K. A. Whittaker, J. Keaveney, I. G. Hughes, A. Sargsyan, D. Sarkisyan, and C. S. Adams, Spectroscopic detection of atom-surface interactions in an atomic-vapor layer with nanoscale thickness, [Phys. Rev. A](#) **92**, 052706 (2015).